

# Numerical Investigation of Scaling Properties of Turbulent Premixed Flames

Jens C. Niemeyer  
Max-Planck-Institut für Astrophysik  
Karl-Schwarzschild-Str. 1  
85740 Garching, Germany

and

Alan R. Kerstein  
Combustion Research Facility  
Sandia National Laboratories  
Livermore, CA 94551-0969, USA

April 19, 2018

## Abstract

Gibson scaling and related properties of flame-surface geometry in turbulent premixed combustion are demonstrated using a novel computational model, Deterministic Turbulent Mixing (DTM). In DTM, turbulent advection is represented by a sequence of maps applied to the computational domain. The structure of the mapping sequence incorporates pertinent scaling properties of the turbulent cascade. Here, combustion in Kolmogorov turbulence (kinetic-energy cascade) and in Bolgiano-Obukhov convective turbulence (potential-energy cascade) is simulated. Implications with regard to chemical flames and astrophysical (thermonuclear) flames are noted.

# 1 INTRODUCTION

A widely recognized paradigm of turbulent premixed combustion is the propagation of a dynamically passive, advected surface at fixed speed  $u_0$  relative to the fluid. Despite the omission of important flame-turbulence interactions such as flame-generated turbulence and stretch-induced variation of the laminar flame speed  $u_0$ , scaling properties deduced from this formulation have proven useful for the interpretation of turbulent combustion processes.

Based on the passive-surface picture, three interrelated scaling properties that describe the structure and evolution of turbulent premixed flames (here considering only the flamelet combustion regime) have been proposed, and the predictions have been compared to measurements. First, a scale-invariant law governing the dependence of  $u_T/u_0$  on  $u'/u_0$ , where  $u_T$  is the turbulent burning velocity and  $u'$  is the root-mean-square turbulent velocity fluctuation, has been derived and confirmed experimentally (Pocheau and Queiros-Condé, 1996). In particular, this law conforms to the dimensionally mandated scaling  $u_T \sim u'$  for  $u' \gg u_0$ . Second, measurements of the flame-surface fractal dimension (North and Santavicca, 1990) are consistent with the scaling prediction (Kerstein, 1988)  $D = 7/3$ . Third, it has been proposed that flame-surface fluctuations are suppressed below a length scale  $l_g$  at which the generation of fluctuations by turbulence and smoothing of fluctuations by flame propagation are in balance. The balance scale  $l_g$  is determined by setting the eddy velocity equal to  $u_0$ . The inertial-range scaling

$$\tau(l) \sim \left(\frac{l}{L}\right)^{2/3} \frac{L}{u'} \quad (1)$$

of the turnover time  $\tau(l)$  of size- $l$  eddies is invoked, where  $L$  is the turbulence integral scale and  $u'$  is the rms velocity fluctuation. Taking  $l/\tau(l)$ , to be the size- $l$  eddy velocity,  $l_g$  is determined from  $l_g/\tau(l_g) = u_0$ , yielding the Gibson scaling (Peters, 1988)

$$l_g/L \sim (u_0/u')^3. \quad (2)$$

Measured flame structure does not obey this scaling. Rather, the available data suggests that lower-cutoff behavior is sensitive to flame-turbulence interactions omitted from the passive-surface picture (North and Santavicca, 1990; Gülder and Smallwood, 1995; Erard *et al.*, 1996).

These three scalings are interrelated in that any two of them imply the third, as demonstrated in Sec. 3.1. In this regard, the failure of Gibson scaling despite the confirmation of the other scalings has not been explained. The approach taken here to address this conundrum is to construct an idealized numerical model of dynamically passive, propagating interfaces advected by turbulence, formulated so that all three scalings are necessarily obeyed in the limit  $u' \gg u_0$ . The model is used to investigate the transition to the asymptotic behaviors as  $u'/u_0$  increases. The numerical results suggest an interpretation of the experimental results in terms of the influence of flame-turbulence interactions and finite- $u'/u_0$  effects.

The discussion thus far is specific to the kinetic-energy cascade in incompressible, constant-density turbulence, governed by the Kolmogorov scaling, Eq. (1). This is the cascade generated by large-scale shear applied, e.g., at flow boundaries. In buoyant turbulent flows with unstable stratification, the large-scale energy input is potential energy that is converted to kinetic energy. Potential energy as well as

kinetic energy can cascade to smaller scales, and exchange between potential and kinetic energy can occur at each scale. It has been proposed (L’vov and Falkovich, 1992) that the potential-energy cascade may dominate. This implies the scaling

$$\tau(l) \sim \left(\frac{l}{L}\right)^{2/5} \frac{L}{u'}, \quad (3)$$

consistent with an earlier proposal by Bolgiano and Obukhov in a different context. This ‘Bolgiano-Obukhov’ (BO) scaling is controversial; Borue and Orszag (1997) discuss experimental, computational, and analytical results supporting and contradicting Eq. (3).

Recognizing the considerable if not conclusive support for Eq. (3), numerical results are presented for flame propagation in cascades governed by Eq. (3). The inner-cutoff scale and the fractal dimension of flames in BO turbulence are predicted from scaling and compared to numerical results. Though this regime is of some relevance to chemical combustion, the principal motivation is thermonuclear combustion in supernovae. Implications in this regard are noted.

## 2 METHOD

### 2.1 General Technique

A new computational model, Deterministic Turbulent Mixing (DTM), is formulated for the study of multiscale phenomena of interfaces propagating in stirred media. Its spirit is to achieve maximum spatial resolution by a radical simplification of specific physical mixing processes, e.g., fully developed hydrodynamic turbulence. In particular, mixing is characterized here only by a universal mapping procedure for every length scale and by the relative frequency of mapping events. Since interface propagation can be implemented as a discrete binary process, a method that fulfills the above description is conveniently based on a cellular grid of discrete binary states, henceforth termed ‘unburned’ and ‘burned’ in analogy with turbulent flame propagation. Furthermore, we have the freedom to choose the spectral distribution of mixing events directly and can therefore restrict the calculation to two spatial dimensions without being constrained by inverse cascade effects of two-dimensional turbulence. The method is also applicable in three dimensions, but this is not implemented here.

The computational domain is a two-dimensional ( $N \times N$ ) square grid of cells of size  $(\Delta x)^2$ , where  $N = 2^r$ . Every computation starts with the lower half of the domain ‘burned’ and the upper half ‘unburned’. The algorithm of DTM can then be sketched as follows: during each burning time step  $\tau_{\text{burn}}$ , every neighboring fuel cell of a previously burned cell is burned, mimicking laminar interface propagation with a speed  $u_0 = \Delta x / \tau_{\text{burn}}$ . Here, horizontal, vertical, and diagonal neighbors are included. For convenience, we assign  $\Delta x = \tau_{\text{burn}} = 1$  and therefore  $u_0 = 1$ . Note that only the relative frequency of mixing and burning events is dynamically relevant, i.e., the normalization of time and length scales is arbitrary.

Mixing is implemented as a series of discrete events which map the entire grid onto itself. Each map  $\mathcal{M}_i$  convolutes the interface on a characteristic length scale  $l_i = 2^i$ , where  $i_{\text{min}} \leq i \leq i_{\text{max}} < r$ . A

sequence of maps involving  $l_i$  values spanning a large dynamic range leads to a highly complex, multiscale interface structure. A time scale  $\tau_i = \tau(l_i)$  regulates the frequency of mapping events on the scale  $l_i$  relative to the interface propagation time step  $\tau_{\text{burn}}$ . This function relating the time and length scales of the problem is the only link to hydrodynamic turbulence; for instance, by choosing a power law dependence of  $\tau_i$  on  $l_i$  we can model different scaling regimes for the turbulent velocities. The goal of DTM is to study interface properties subject to various rules for  $\tau_i$  and rather generic forms for  $\mathcal{M}_i$ . In this approach, complexity arises from a purely deterministic multiscale mixing process coupled to local interface propagation. No random elements are involved.

Owing to the absence of floating-point operations, the computational expense for all the described steps is relatively low. Limited mainly by memory considerations, a large dynamic range can be achieved and the evolution can easily be followed over many large scale dynamical times  $\tau_{i_{\text{max}}}$ . Identification of the largest mixing scale  $l_{\text{max}} = 2^{i_{\text{max}}}$  with the integral scale  $L$  and the minimum scale  $l_{\text{min}} = 2^{i_{\text{min}}}$  with the Kolmogorov dissipation scale  $l_k$  yields an estimate for the effective turbulent Reynolds number of the Kolmogorov-cascade computations,

$$Re = \left(\frac{L}{l_k}\right)^{4/3} = 2^{4 \Delta i / 3}, \quad (4)$$

with  $\Delta i = i_{\text{max}} - i_{\text{min}}$ . Calculations reported here involve  $\Delta i = 9$ , corresponding to  $Re \approx 4100$  for the Kolmogorov cascade.

On the other hand, this brief description also shows the main restrictions of DTM. First of all, local interface propagation is completely independent of the mixing process. Strain effects on  $u_0$  are omitted. Furthermore, feedback of ‘burning’ onto the  $\mathcal{M}_i$  and  $\tau_i$  is not represented. In particular, there is no flame-generated turbulence. Most importantly, the maps  $\mathcal{M}_i$  are purely artificial and are not claimed to reproduce detailed mixing dynamics of hydrodynamic turbulence. They can be expected, however, to belong to the same universality class as a large ensemble of scale invariant turbulent eddies, and thus provide useful insight into the statistical behavior of stirred propagating interfaces.

## 2.2 Implementation of Mixing

Given the general philosophy of DTM as described above, the following mixing properties can be varied according to the physical system under consideration: the form of the maps  $\mathcal{M}_i = \mathcal{M}(l_i)$ , the mapping frequencies  $\tau_i^{-1} = \tau^{-1}(l_i)$  (equivalent to choosing a power spectrum of a stochastic mixing process), and their normalization with respect to the local interface propagation speed  $u_0$ .

We shall first describe the procedure for mixing on a single length scale  $l_i$  for a given frequency  $\tau_i^{-1}$ . The choice of  $\mathcal{M}_i$  is the least constrained from first principles. Features that should be incorporated into discrete maps in reduced turbulence models have been summarized (Kerstein, 1991). By construction, their effect is intended to be a combined stretching and folding of the interface on the length scale  $l_i$ . Consequently, they contain the single parameter  $l_i$ , and their dependence on the spatial coordinates is preferably chosen to be continuous and differentiable in order to reflect smooth physical mixing.

As a specific representation for  $\mathcal{M}_i$ , we choose a sinusoidal deformation of the entire grid, analogous to the action of a single Fourier mode. For a given length scale  $l_i$ , the sequence of maps alternates between deformation in the  $x$  and  $y$  directions. The time between successive maps for given  $l_i$  is  $\tau_i$ . Then for given  $l_i$ , the mapping sequence is:

$$\mathcal{M}_i(n) : \{x, y\} \rightarrow \begin{cases} \{x, y + \text{int}[l_i \sin(\pi x/2l_i)]\} & \text{if } t = 2n \tau_i \\ \{x + \text{int}[l_i \sin(\pi y/2l_i)], y\} & \text{if } t = (2n + 1) \tau_i \end{cases} \quad (5)$$

for  $n = 0, 1, \dots$ , where  $t$  denotes the epochs at which the indicated maps are implemented and  $\text{int}[\cdot]$  stands for the nearest integer. Periodic boundary conditions are imposed horizontally, and we assume completely burned or unburned material at the bottom and top boundaries, respectively. The computational domain is shifted vertically as needed to prevent burned material from contacting the top boundary.

Figure 1 demonstrates the effect of the alternating  $x$  and  $y$ -maps, Eq. (5), for a single length scale  $l_i = r - 3$  over a time period of  $6 \tau_i$ . Here, burning is not implemented. Starting with a planar interface, the  $\mathcal{M}_i$  deform it step by step into rolls resembling vortices of a Kelvin-Helmholtz (KH) unstable shear layer. Maps acting on multiple length scales can thus be envisioned to produce a superposition of KH vortices on all scales.

This picture is specific to the mathematical definition, Eq. (5), of the mapping sequence. In particular, Eq. (5) is formulated so that the point  $(0, 0)$  and its periodic images never move. If successive mappings are allowed to have different sets of fixed points, more complicated patterns can be obtained for fixed  $l_i$ . The intent here is to obtain the simplest possible behavior for fixed  $l_i$  so that multiscale structure mainly reflects the assumed distribution of  $l_i$ . For purposes such as the study of flame surface response to local turbulence structure, some variant of this formulation might be preferable. A three-dimensional formulation can readily be configured to generate helical fluid paths, reminiscent of flow near vortex tubes. Any such analogy between the model and properties of turbulent flow would require detailed validation that has not yet been undertaken. The intent here is to formulate a model that emulates particular scaling properties of propagating surfaces advected by turbulence, irrespective of possible broader implications of the model.

Generalization to multiple length scales is achieved by concurrent implementation of the map sequences  $\mathcal{M}_i(n)$  consecutively for all  $i \in [i_{\min}, i_{\max}]$ . If events corresponding to more than one scale  $i$  occur at a given epoch, then the events are implemented in order of increasing  $i$ . (Smaller-scale events are governed by shorter time scales and therefore are deemed to be ‘completed’ before concurrent larger-scale events. Scaling properties are insensitive to this somewhat arbitrary interpretation.) The dependence of the event frequency on  $l_i$  is derived from the notion of a velocity spectrum  $v_i = v(l_i)$  of turbulent fluctuations in scale space. We define

$$\tau_i = \frac{l_i}{v_i} \quad (6)$$

in analogy with the turnover time of size- $l_i$  eddies. By postulating a power law for the velocity distribution in scale space,

$$v_i \propto \left(\frac{l_i}{\lambda}\right)^\eta V, \quad (7)$$

where  $\lambda$  and  $V$  are reference length and velocity scales (analogous to the turbulence integral scale and rms velocity fluctuation), we can link the inverse mapping frequencies (the time between two consecutive mapping events) directly to the length scales:

$$\tau_i \propto \left(\frac{l_i}{\lambda}\right)^{1-\eta} \frac{\lambda}{V}. \quad (8)$$

Unless otherwise noted, we will henceforth set  $\eta = 1/3$ , relating the DTM mixing process specifically to inertial-range Kolmogorov turbulence.

In order to normalize the mixing frequencies with respect to the interface propagation, the parameter

$$z = \frac{u_0 \tau(l_k)}{l_k} \quad (9)$$

is introduced. As in Eq. (4), the smallest mixing scale  $l_{i_{\min}}$  is interpreted as the dissipation scale  $l_k$ . In the derivation of Eq. (2) it was assumed that inertial-range scaling applies at the scale  $l_g$ , and thus that  $l_g > l_k$ . This is equivalent to the requirement  $z > 1$ . In all of our calculations,  $z \geq 2$ .

$z$  parameterizes the small-scale mixing. The large-scale mixing is parameterized by  $u'/u_0$ , which is defined in the DTM context as  $u'/u_0 = L/[u_0 \tau(L)]$ , where the largest mixing scale  $l_{i_{\max}}$  is interpreted as the turbulence integral scale  $L$ . This definition omits the contribution of mixing at scales below  $L$ . A more literal analog of the turbulent velocity fluctuation  $u'$  can be defined within DTM. The choice of definition rescales the numerical results, but does not affect the properties of interest here.

Based on Eq. (4), these parameters obey the relation  $zu'/u_0 = Re^{1/4}$  for the Kolmogorov cascade. The turbulent combustion process can thus be parameterized by  $u'/u_0$  and either  $Re$  (the usual choice) or  $z$ .  $z$  is convenient for identifying the range of validity of Gibson scaling, and therefore is adopted here. For all Kolmogorov-cascade computations reported here,  $Re = 2^{12}$ , so  $u'/u_0 = 8/z$ .

Common parameters of all computations (except an illustrative case shown in Figure 2) were the grid size,  $N = 2^{12}$ , and the indices  $i_{\min} = 1$  and  $i_{\max} = 10$  determining the scales  $l_k = 2^{i_{\min}}$  and  $L = 2^{i_{\max}}$  of the smallest and largest maps.  $z$  ranged from 2 to 4, yielding  $2 < u'/u_0 < 4$  for the Kolmogorov cascade. For the Bolgiano-Obukhov cascade, this  $z$  range corresponds to  $10.5 < u'/u_0 < 21$ .

Figure 2 shows a typical flame image from a computation based on the Kolmogorov scaling. The multiscale nature of the flame interface is apparent.

## 3 RESULTS AND INTERPRETATIONS

### 3.1 Kolmogorov Inertial-Range Turbulence

Here, DTM is used to investigate the interface properties that can be quantified in terms of the box-counting statistics described by Menon and Kerstein (1992). This is implemented by partitioning the flame image into square boxes with side lengths  $l_j = 2^j$ ,  $j = 0 \dots r - 2$  and counting the number  $b(l_j)$  of boxes that contain at least one newly burned cell. Obviously,  $b(l_0)$  is the total number of newly burned cells, so  $u_T/u_0$  is the ensemble average of  $b(l_0)/N$ , where  $b(l_0)/N$  may be interpreted geometrically as the

interface arc length per unit transverse length. Accordingly,  $A_j = l_j b(l_j)/(l_0 N)$  may be interpreted as the arc length per unit transverse length of the smoothed interface, for smoothing scale  $l_j$ . Henceforth,  $A_j$  is denoted  $A(l)$ , omitting the subscript on  $l$ .

If  $l$  is much smaller than the finest scale of surface wrinkling, then the smoothing has no effect, so  $A(l)$  should converge to a constant value in the limit of small  $l$ . The flattening of computed profiles of this quantity at small  $l$  is seen in Figure 3.

For  $l$  much larger than the flame-brush thickness, the smoothed interface is planar, so  $A(l)$  converges to unity. The computational domain is not large enough to demonstrate this asymptote, but this is immaterial because the unity asymptote is a mathematical necessity. More significant is the tendency for the profiles to collapse with respect to  $l/L$  with increasing  $l$ . This indicates that the flame-brush thickness scales as  $L$ .

Interpreting the two-dimensional computation as a planar cut through three-dimensional space, fractal scaling implies  $A(l) \sim l^{2-D}$ , where  $D$  is the fractal dimension of the flame surface in three-dimensional space (North and Santavicca, 1990). This scaling is identified by linear dependence on a log-log plot of  $A(l)$ .

The profiles in Figure 3 suggest linear scaling between the inner and outer cutoffs. The linear range appears to broaden with increasing  $u'/u_0$  (corresponding to decreasing  $z$ ), as one would expect. The slope increases with  $u'/u_0$ , and in fact, the implied fractal dimensions fall within the error bars on a plot of measured  $D$  as a function of  $u'/u_0$  (North and Santavicca, 1990). The predicted value  $D = 7/3$  is not attained by the computed profiles, consistent with the experimental finding that this occurs only for  $u'/u_0$  much higher than the computed cases (North and Santavicca, 1990).

Next, it is shown that any two of the three scalings discussed in the Introduction imply the third. Consider a box-counting profile, plotted in the format of Figure 3, for  $u'/u_0 \gg 1$ . For  $l \ll l_g$ , it approaches a plateau level of order  $u'/u_0$  because  $u_T \sim u'$ . For  $l \gg L$ , it approaches a plateau level of unity. Implicit here is the assumption that the flame-brush thickness is of order  $L$ . However, this is not an additional assumption. Rather, this assumption and  $u_T \sim u'$  both follow from the assumption that flame-brush length and time scales are governed by large-eddy length and time scales for  $u' \gg u_0$ .

Thus, the ratio of the small- $l$  and large- $l$  levels is  $u'/u_0$ . In Figure 3, this vertical span is traversed over a horizontal span  $L/l_g$ . If there is fractal scaling, then the profile has a region of linear dependence between these limits. In the limit  $u' \gg u_0$ , the slope  $2 - D$  of this linear region, based on these estimates, is  $-\log(u'/u_0)/\log(L/l_g)$ . This gives  $l_g/L \sim (u_0/u')^{1/(D-2)}$ , showing that the fractal scaling implies the Gibson scaling and vice versa. Analogous reasoning shows that if both scalings are obeyed, then  $u_T \sim u'$ .

The apparent implication of the computed results in Figure 3 and of the measurements is that fractal scaling is more robust than Gibson scaling, because fractal scaling is obtained, but for  $D$  values inconsistent with Gibson scaling. However, a different picture is obtained when  $Au_0/u'$  is plotted with respect a Gibson-normalized horizontal axis, as in Figure 4. Here,  $l_g$  is defined as  $(u_0/u')^3 L$ . In this format, Gibson scaling, in conjunction with  $u_T \sim u'$ , implies collapse of profiles below the outer cutoff.  $u_T \sim u'$  by itself implies only a collapse of the low- $l$  plateau levels. The profiles indicate some deviation from the

latter collapse, suggesting either deviation from this scaling in the  $u'/u_0$  range of the computations, or numerical resolution effects. Resolution effects can be discounted only if the computations resolve the low- $l$  plateau over a significant  $l$  range. It is evident that the resolution is marginal by this criterion.

Whatever the source of low- $l$  deviation, the collapse between the inner and outer cutoffs indicates accurate conformance to Gibson scaling. It is also evident that the universal scaling function thereby obtained has significant curvature throughout the range in which it is well resolved. Although an eventual transition to fractal scaling with  $D = 7/3$  is a necessary consequence of the convergence of the profiles to a universal form (and the assumption that the outer cutoff scales as  $L$ ), it appears that the transition from the low- $l$  plateau to the fractal scaling extends over more than three decades of  $l$ .

Thus, Figure 4 indicates that both the Gibson scaling and the relation  $u_T \sim u'$  are more robust than fractal scaling because they are both seen at  $u'/u_0$  for which the latter is not seen. How can this be reconciled with Figure 3, and with measurements?

The apparent linear regions in Figure 3 may be manifestations of the inflection points of the profiles, which necessarily occur owing to profile flattening at small and large  $l$ . Measured profiles used to infer fractal dimensions typically have no greater range of apparent linearity, oftentimes less. Comparison of Figures 3 and 4 shows that extraction of fractal dimensions from such data is problematic. A more reliable method for determining scaling properties is to demonstrate that a particular scaling collapses a family of curves parameterized by  $u'/u_0$ .

Onset of fractal scaling may be slow because the mathematical requirement of spatial homogeneity is not strictly obeyed. Flame geometry varies with streamwise location. For example, isolated pockets of unburned material are more likely to be found on the upstream side of the flame brush (e.g., Figure 2). Therefore, flame geometry is approximately fractal only when the flame interface near the flame-brush center becomes so wrinkled that it dominates the box-occupancy statistics over a significant dynamic range. In this case, local homogeneity near the flame-brush center is sufficient for approximate fractal behavior. This condition can be fulfilled only for high  $u'/u_0$ .

In contrast, Gibson scaling reflects the local balance between wrinkling by advection and smoothing by propagation. Because DTM has been formulated so that propagation and advection are both spatially homogeneous, this scaling should not vary with streamwise location. This expectation is supported by the apparent robustness of Gibson scaling. However, in combustion processes with flame-turbulence interactions such as flame-generated turbulence, turbulence intensity will, in general, vary with streamwise location relative to the flame brush, so the onset of Gibson scaling may be inhibited.

## 3.2 Convective Turbulence

DTM allows freedom of choice for the assumed turbulent velocity spectrum. The impact of a particular cascade mechanism on turbulent flame propagation is investigated by fixing the parameter  $\eta$  in equation (7) to the relevant scaling exponent. We used  $\eta = 1/3$  in the calculations summarized in Sec. 3.1.

A particular example of an eddy cascade whose velocity scaling exponent differs from  $\eta = 1/3$  is buoyancy-driven turbulence. As indicated in Sec. 1, the coupled density and velocity cascades are



presumed to be governed by the Bolgiano-Obukhov (BO) scaling  $\eta = 3/5$ . The scaling properties of premixed flames propagating in buoyancy-driven flows are derived on this basis. Following the arguments of Kerstein (1988), we expect a fractal dimension of  $D_{\text{BO}} = 2\frac{3}{5}$ . The lower cutoff scale, denoted  $l_w$ , is the balance scale at which the eddy velocity  $(l/L)^\eta u'$  is of order  $u_0$ , giving

$$l_w = (u_0/u')^{5/3} L . \quad (10)$$

DTM provides a simple illustration of the above relations. The results of computations with  $\eta = 3/5$  are shown in Figure 5. They involved  $z = 2, 3$ , and  $4$ , corresponding to  $u'/u_0 = 21, 14$ , and  $10.5$ . The format of Figure 4 is used, except that  $l$  is normalized by  $l_w$  in order to demonstrate the BO analog of Gibson scaling. Collapse of the computed profiles verifies this scaling. As in Figure 4, it is seen that there is a gradual transition to the anticipated fractal scaling.

These results have significant implications in the context of astrophysics. A specific class of extremely bright astronomical events, so-called Type Ia supernovae, can be consistently explained by thermonuclear explosions of compact white dwarf stars (Niemeyer and Woosley, 1997, and references therein). In this scenario, the thermonuclear reaction wave propagates from the stellar core outwards as a microscopically thin flame sheet, ‘burning’ carbon and oxygen to iron-group elements. The resulting stratification of hot, burned material underneath the dense outer layers is Rayleigh-Taylor unstable, rapidly giving rise to the production of strong turbulence. Hence, the situation fulfills all of the criteria for flame propagation in buoyancy-driven turbulence and, consequently, our results obtained for the BO cascade apply. This question is subject to ongoing research; a more detailed analysis will be presented elsewhere (Niemeyer and Kerstein, 1997).

## 4 CONCLUSIONS

Previous work has shown that analysis of a dynamically passive, propagating surface advected by turbulence is a useful framework for interpreting turbulent combustion phenomena. Here, the assumptions generally adopted in this framework have been embodied in a computational model, Deterministic Turbulent Mixing (DTM).

The model provides an explicit numerical demonstration of the scalings governing turbulent premixed flame structure and burning velocity in the flamelet regime. Moreover this demonstration has several implications with regard to turbulent combustion measurements. The main results and conclusions are as follows.

First, the Gibson scaling of the inner cutoff of flame structure in Kolmogorov turbulence is demonstrated by obtaining the collapse of a family of box-occupancy profiles, parameterized by  $u'/u_0$ , with appropriate normalization. This is the first explicit demonstration that Gibson scaling of a propagating surface follows directly from Kolmogorov scaling of turbulent advection.

Second, the structure of the universal scaling function revealed by this collapse is compared to the structure of individual profiles. Though individual profiles suggest fractal scaling with fractal dimension

$D$  that increases with  $u'/u_0$ , the universal function shows no fractal scaling over the scale range probed by the computation. In effect, the different  $D$  values of the individual curves reflect the fact that each individual curve corresponds to a slightly different range, in the Gibson-normalized coordinate, of the universal curve. Thus, the apparent  $u'/u_0$  dependence of  $D$  is a measure of the curvature of the universal function.

Third, the results have bearing on the interpretation of turbulent combustion measurements despite the simplifications inherent in the model. The results indicate that the measured  $u'/u_0$  dependence of  $D$  may in fact be an indication of lack of fractal scaling, rather than variation of a scaling exponent. Measurements suggest eventual convergence to  $D = 7/3$ , but convincing convergence is not attained over a significant dynamic range of  $u'/u_0$ . Thus, one possible explanation of the empirical failure of Gibson scaling is that  $u'/u_0$  large enough to observe the scaling has not yet been achieved in the experiments. However, model results suggest that Gibson scaling, in the passive-surface framework, is more robust than fractal scaling. This suggests that a more likely explanation of Gibson-scaling failure is flame-turbulence interactions omitted from the passive-surface formulation. If this is true, then the convergence to  $D = 7/3$ , if it occurs, may reflect a combination of flame-turbulence interaction effects rather than applicability of the scaling analysis.

Fourth, the model demonstrates the proposed connection between turbulence structure and flame structure. When the Bolgiano-Obukhov scaling presumed to govern convective turbulence is adopted in lieu of the Kolmogorov scaling, the inner-cutoff scaling changes accordingly. The analysis implies a corresponding change of  $D$ , but this cannot be demonstrated within the computationally accessible range of scales. It is interesting to note that the passive-surface modeling framework may be more relevant to buoyancy-driven thermonuclear flames than to chemical flames because the astrophysical flames have relatively low thermal expansion, hence weak flame-turbulence interactions (except for gravitational forcing), and because  $u'/u_0$  in these flames is 'astronomical.'

## 5 ACKNOWLEDGMENTS

The authors would like to thank R. Rinne for facilitating this collaboration and S. Woosley for consenting to the use of his initial. This research was partially supported by the Division of Engineering and Geosciences, Office of Basic Energy Sciences, U.S. Department of Energy. The computations were performed at the Rechenzentrum Garching, Germany.

## References

- [1] Borue, V., and Orszag, S. A. (1997) Turbulent convection driven by a constant temperature gradient. Preprint.
- [2] Erard, V., Boukhalfa, A., Puechberty, D., and Trinité, M. (1996) A statistical study on surface properties of freely-propagating turbulent premixed flames. *Combust. Sci. Tech.* **113**, 313.
- [3] Gülder, O. L., and Smallwood, G. J. (1995) Inner cutoff scale of flame surface wrinkling in turbulent premixed flames. *Combust. Flame* **103**, 107.
- [4] Kerstein, A. R. (1988) Fractal dimension of turbulent premixed flames. *Combust. Sci. Tech.* **60**, 441.
- [5] Kerstein, A. R. (1991) Linear-eddy modelling of turbulent transport. Part 6. Microstructure of diffusive scalar mixing fields. *J. Fluid Mech.* **231**, 361.
- [6] L'vov, V. S., and Falkovich, G. E. (1992) Conservation laws and two-flux spectra of hydrodynamic convective turbulence. *Physica D* **57**, 85.
- [7] Menon, S., and Kerstein, A. R. (1992) Stochastic simulation of the structure and propagation rate of turbulent premixed flames. *Twenty-Fourth Sympos. (Intl.) on Combustion*, p. 443.
- [8] Niemeyer, J. C., & Kerstein, A.R. (1997) Burning regimes of nuclear flames in SN Ia explosions. *New Astronomy*, in press<sup>1</sup>.
- [9] Niemeyer, J. C., & Woosley, S. E. (1997) The thermonuclear explosion of Chandrasekhar mass white dwarfs. *Astrophys. J.* **475**, 740.
- [10] North, G. L., and Santavica, D. A. (1990) The fractal nature of turbulent premixed flames. *Combust. Sci. Tech.* **72**, 215.
- [11] Peters N. (1988) Laminar flamelet concepts in turbulent combustion. *Twenty-First Sympos. (Intl.) on Combustion*, p. 1231.
- [12] Pocheau, A., and Queiros-Condé, D. (1996) Scale covariance of the wrinkling law of turbulent propagating interfaces. *Phys. Rev. Lett.* **76**, 3352.

---

<sup>1</sup>also available at [http://www.mpa-garching.mpg.de/~jcn/pub\\_flame.html](http://www.mpa-garching.mpg.de/~jcn/pub_flame.html)

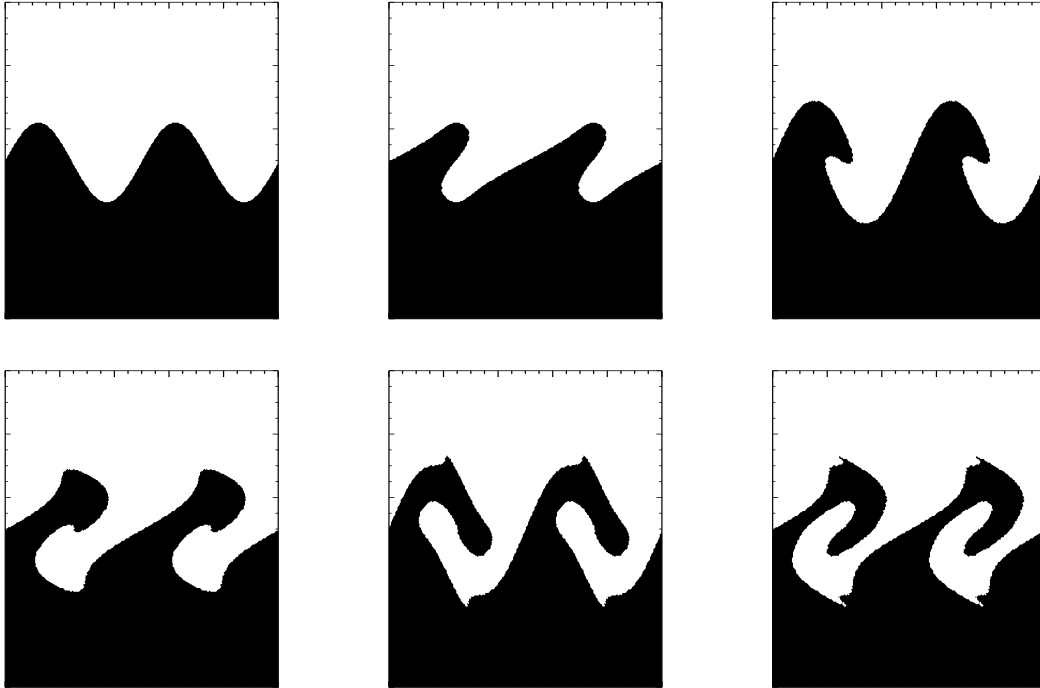


Figure 1: Snapshots of the interface during the first 6 iterations of the alternating mapping sequence, Eq. (5). For this demonstration, only a single length scale,  $l_i = 32$ , was mapped and interface propagation was turned off. The resolution was  $N = 2^8$ . The sense of rotation can be reversed by changing  $+$  to  $-$  in either the top or the bottom line of Eq. (5)

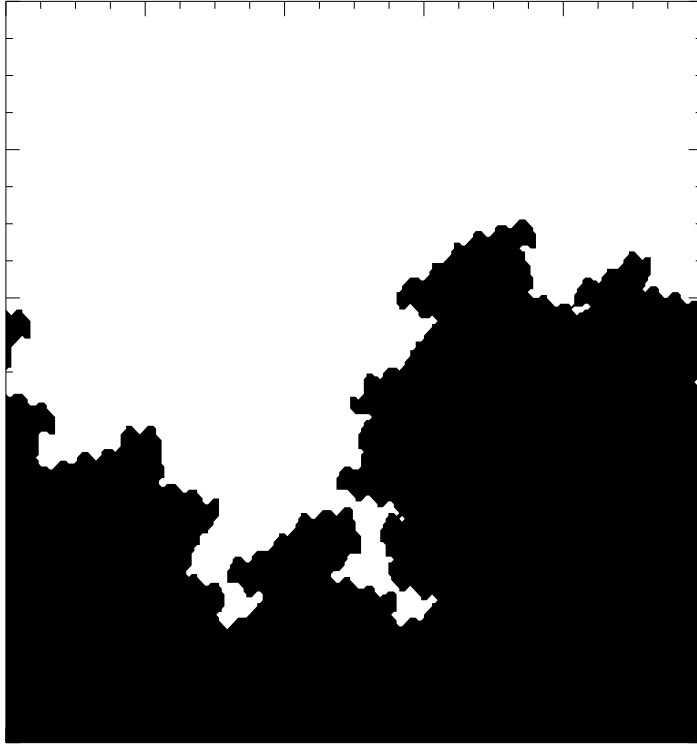


Figure 2: Image of a flame in a simulated Kolmogorov cascade after  $\approx 30$  large scale mapping times. Black is burned. The computation used  $N = 2^8$ ,  $i_{\min} = 1$ ,  $i_{\max} = 6$ , and  $z = 1$ .

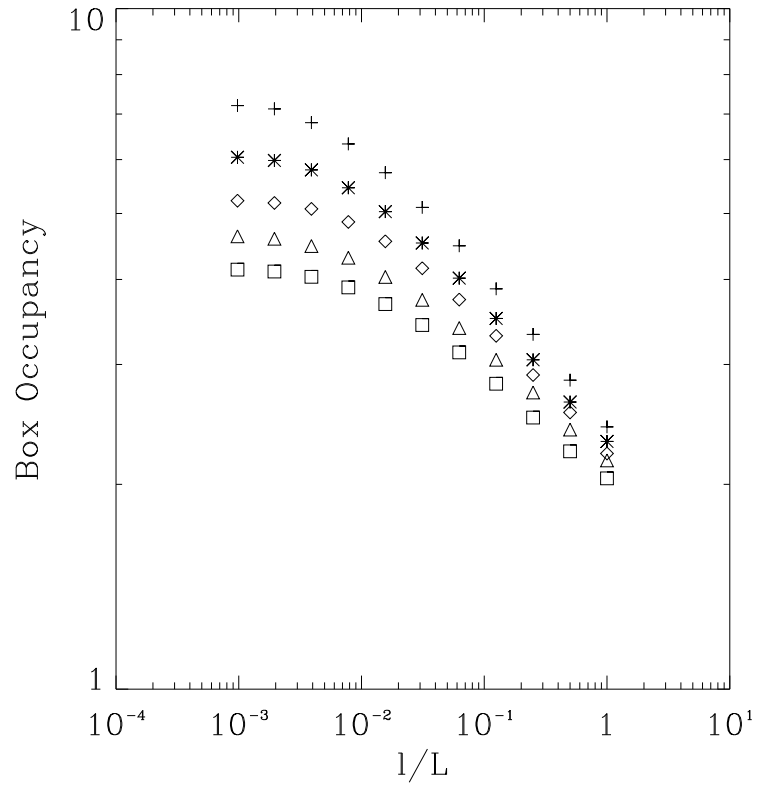


Figure 3: Normalized box occupancy  $A$  as a function of length scale, normalized to the integral scale  $L$ . The symbols represent, from top to bottom:  $z = 2, 2.5, 3, 3.5, 4$ .

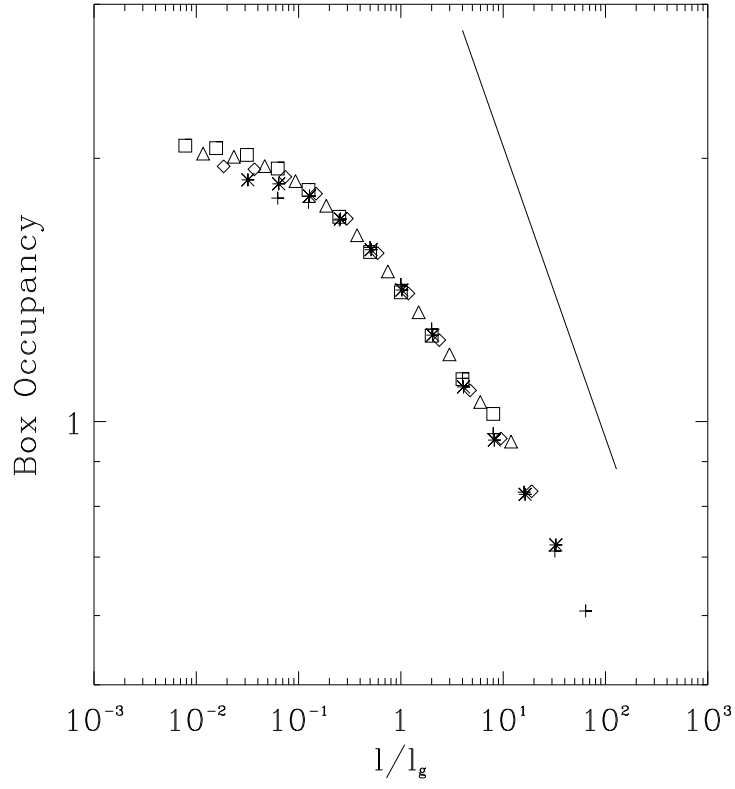


Figure 4: Rescaled box occupancy  $Au_0/u'$  as a function of length scale, normalized to the Gibson scale  $l_g$ . The correspondence between symbols and  $z$  values is as in figure 3. The line corresponds to a linear decline with a slope of  $-1/3$ .

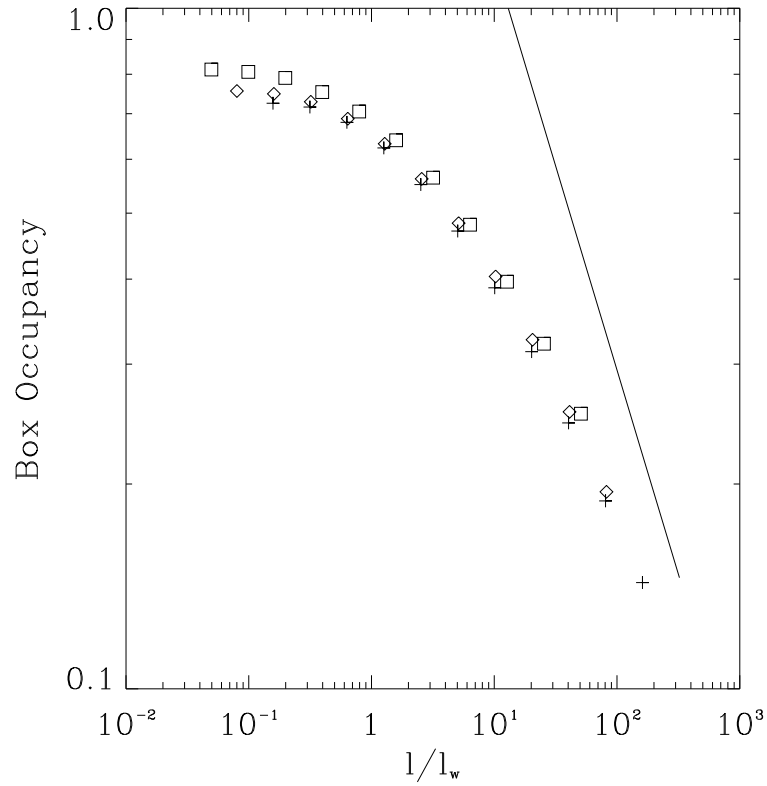


Figure 5: Rescaled box occupancy  $Au_0/u'$  in convective turbulence (eddy-velocity scaling exponent  $\eta = 5/3$ ) as a function of length scale, normalized to the cutoff scale  $l_w$ . The correspondence between symbols and  $z$  values is as in figure 3. The line corresponds to a linear decline with a slope of  $-3/5$ .